CCS Chemistry

RESEARCH ARTICLE

Received: June 24, 2024 | Accepted: Aug. 13, 2024 | Published: Sept. 16, 2024

Heterogenization of a Dinuclear Cobalt Molecular Catalyst in Porous Polymers via Covalent Strategy for CO_2 Photoreduction with Record CO Production Efficiency

Yun-Nan Gong[1], Si-Ya Lv[1], Hao-Yu Yang[1], Wen-Jie Shi[1], Jing-Jing Wang[1], Long Jiang[2], Di-Chang Zhong[1]* & Tong-Bu Lu[1]*

[1]*MOE International Joint Laboratory of Materials Microstructure, Institute for New Energy Materials and Low Carbon Technologies, School of Materials Science and Engineering, Tianjin University of Technology, Tianjin 300384,* [2]*Instrumental Analysis and Research Center, Sun Yat-Sen University, Guangzhou 510275*

**Corresponding authors: dczhong@email.tjut.edu.cn; lutongbu@tjut.edu.cn*

Cite this: *CCS Chem.* **2024**, 6, 3030–3040
DOI: 10.31635/ccschem.024.202404675

Photocatalytic CO_2 reduction into chemical fuels is a promising route for alleviating the energy crisis and environmental issues. However, reported catalysts still exhibit low catalytic efficiencies, which hinders the development of this important reaction. Herein, we report the heterogenization of a dinuclear cobalt molecular catalyst into two porous polymers (Co_2-P_1 and Co_2-P_2) using a covalent strategy for photocatalytic CO_2 reduction. As a result, Co_2-P_1 with a phenyl group as the linker exhibited high catalytic performance for the photochemical CO_2-to-CO conversion with a CO production rate of 568.8 mmol g^{-1} h^{-1} and turnover frequency (TOF) of 11.6 min^{-1} (CO selectivity, 95.2%). More impressively, by extending the phenyl to biphenyl linker, the resulting Co_2-P_2 shows obviously enhanced photocatalytic efficiency for CO_2 reduction to CO, with a record CO production rate of 1063.0 mmol g^{-1} h^{-1} and TOF of 23.6 min^{-1} (CO selectivity, 94.9%) under a laboratory light source. Furthermore, Co_2-P_2 also shows outstanding catalytic activity for photocatalytic CO_2 reduction under natural sunlight, with a CO production rate of 544.1 mmol g^{-1} h^{-1} and TOF of 12.1 min^{-1} (CO selectivity, 97.2%). Systematic studies demonstrated that fast electron transfer from the photosensitizer to the catalyst greatly contributes to the superior catalytic activity of Co_2-P_2.

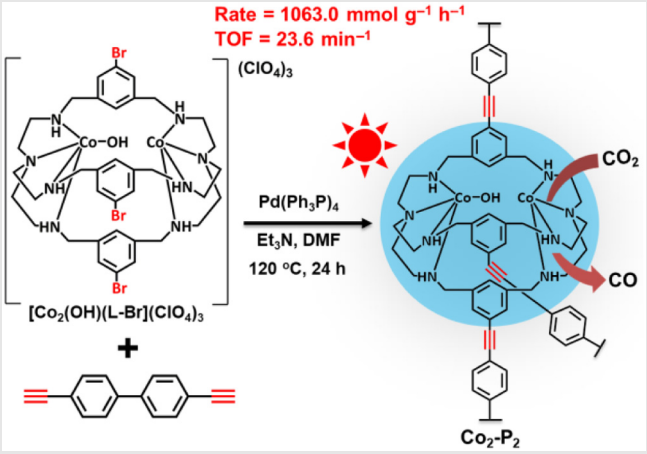

Keywords: molecular catalyst, heterogenization, covalent strategy, polymer, photocatalysis, CO_2 reduction

DOI: 10.31635/ccschem.024.202404675
Citation: *CCS Chem.* **2024**, 6, 3030–3040
Link to VoR: https://doi.org/10.31635/ccschem.024.202404675

Introduction

Photocatalytic CO_2 reduction into chemical fuels has attracted considerable attention because it can not only help to lower the CO_2 concentration in the atmosphere, but also realize economically feasible solar-to-chemical conversion.[1-5] However, the efficient conversion of CO_2 is difficult because of the high kinetic and thermodynamic inertness of CO_2 molecule.[6-10] Thus, it is desirable to develop efficient photocatalysts for this important reaction. Recently, a series of homogeneous and heterogeneous photocatalysts has been designed and synthesized,[11-17] among which homogeneous catalysts usually exhibit excellent catalytic performance because of the high utilization of active sites and fast charge transfer between the photosensitizer and catalytic centers. Nevertheless, it is difficult to separate and reuse homogeneous catalysts from the catalytic system after reaction.[11-14] In contrast, heterogeneous catalysts can be easily separated and recycled,[15-17] which are more beneficial for practical industrial applications.

Over the past several decades, a variety of porous materials such as inorganic semiconductors, metal–organic frameworks, and organic polymers have been developed for heterogeneous photochemical CO_2-to-CO conversion.[18-20] Although great progress has been achieved, most of these porous materials still exhibit low catalytic efficiency, with a CO production rate of <100 mmol g^{-1} h^{-1} or turnover frequency (TOF) value of <1.0 min^{-1}.[21-34] This may be attributed to the low utilization of active sites and/or poor charge transfer efficiency between the photosensitizer and catalytic centers. To overcome these problems, the heterogenization of homogeneous molecular catalysts into porous heterogeneous catalysts would be a facile and effective strategy because they have the capability of encapsulating photosensitizers inside the pores to shorten the charge migration path, thereby improving the charge transfer efficiency.[35-39] As a type of splendid homogeneous molecular catalyst, dinuclear metal complexes with suitable metal···metal separations and spatial configurations have exhibited outstanding catalytic activity for CO_2 photoreduction owing to the dinuclear metal synergistic catalysis effect. Typical examples of dinuclear **CoCo**, **CoZn**, and **NiNi** complexes display superior performance for photochemical CO_2-to-CO conversion.[40-44] Therefore, the heterogenization of these dinuclear metal molecular catalysts into porous heterogeneous catalysts is expected to achieve efficient photocatalytic CO_2 reduction, although related reports are still scarce.

With the above considerations in mind, we successfully synthesized two new porous polymers (**Co_2-P_1** and **Co_2-P_2**) by the heterogenization of a dinuclear cobalt molecular catalyst via a covalent strategy, which exhibited ultrahigh catalytic efficiency for photochemical CO_2-to-CO conversion. In particular, **Co_2-P_2** with biphenyl as the linker achieved an impressive rate of 1063.0 mmol g^{-1} h^{-1} and a TOF value of 23.6 min^{-1} for CO_2 reduction to CO under a laboratory light source. Moreover, **Co_2-P_2** also exhibited high photocatalytic CO_2 reduction performance under natural sunlight, with a CO generation rate of 544.1 mmol g^{-1} h^{-1} and TOF of 12.1 min^{-1}. To the best of our knowledge, **Co_2-P_2** has the highest catalytic efficiency for CO_2 photoreduction among heterogeneous catalysts reported so far. The high photocatalytic performance of **Co_2-P_2** is attributed to its large pore size, which is beneficial for encapsulating the photosensitizer to accelerate electron transfer from the photosensitizer to the catalytic centers.

Experimental Methods

Synthesis of $[Co_2(OH)(L\text{-}Br)](ClO_4)_3$

First, cryptand (L-Br: $C_{36}H_{51}Br_3N_8$) was synthesized according to a method previously reported.[45] Then, L-Br (200 mg) was dissolved in a mixture solution of dichloromethane (18 mL) and ethanol (80 mL), which was stirred under Ar atmosphere for 15 min at ambient temperature. Afterward, an ethanol solution (3.0 mL) containing $Co(ClO_4)_2 \cdot 6H_2O$ (232 mg) was added to the above solution, which was stirred for 30 min at room temperature. The bottle-green powder of $[Co_2(OH)(L\text{-}Br)](ClO_4)_3$ ($C_{36}H_{52}Br_3Cl_3Co_2N_8O_{13}$) was separated by centrifugation and washed with ethanol and diethyl ether. Yield: 97%.

Synthesis of $[Co_2(O_2COCH_2CH_3)(L\text{-}Br)](ClO_4)_3$

The bottle-green powder of $[Co_2(OH)(L\text{-}Br)](ClO_4)_3$ (1.0 mg) was dissolved in acetonitrile (2.0 mL), followed by slow diffusion of ethanol in air at room temperature. After approximately 10 d, bottle-green crystals of $[Co_2(O_2COCH_2CH_3)(L\text{-}Br)](ClO_4)_3$ ($C_{39}H_{56}Br_3Cl_3Co_2N_8O_{15}$) were obtained (yield: 20%).

Synthesis of dinuclear cobalt polymers

Co_2-P_1, **Co_2-P_2**, **Co_2-P_3**, and **Co_2-P_4** were synthesized via Sonogashira–Hagihara coupling reaction. Typically, $[Co_2(OH)(L\text{-}Br)](ClO_4)_3$ (60 mg), 1,4-diethynylbenzene (7.5 mg), 4,4′-diethynyl-1,1′-biphenyl, 1,3-diethynylbenzene or 4,4′′-diethynyl-1,1′:4′,1′′-terphenyl (12.5 mg) and tetrakis(triphenylphosphine)palladium (34.6 mg) were added in a mixed solvent of dimethylformamide (DMF, 10 mL) and triethylamine (13.2 mL). The mixture was purged with N_2 for 20 min and stirred at 120 °C for 24 h. After cooling to room temperature, precipitates of **Co_2-P_1**, **Co_2-P_2**, **Co_2-P_3**, or **Co_2-P_4** were obtained by centrifugation and washed with DMF and methanol.

DOI: 10.31635/ccschem.024.202404675
Citation: *CCS Chem.* **2024**, 6, 3030–3040
Link to VoR: https://doi.org/10.31635/ccschem.024.202404675

Photocatalytic CO_2 reduction experiments

The photocatalytic CO_2 reduction reaction was conducted under 1 atm of a certain atmosphere (CO_2 and Ar) at 25 °C in a 16 mL reactor containing a heterogeneous catalyst (1.0 mg/L) and homogeneous catalyst (0.75 μM), $[Ru(phen)_3](PF_6)_2$ (0.4 mM), 1,3-dimethyl-2-phenylbenzimidazoline (BIH, 0.025 M), and 5 mL CH_3CN or CH_3CN/ H_2O (*v*/*v* = 4:1). The reaction system was degassed with CO_2 or Ar to remove O_2 and other gases, and irradiated under a Xe lamp (λ ≥ 420 nm, light intensity: 160 mW cm^{-2}) or natural sunlight. The generated gases were analyzed using gas chromatography (GC).

Results and Discussion

The $[Co_2(OH)(L\text{-}Br)](ClO_4)_3$ was prepared by the reaction of cryptand (L-Br) and $Co(ClO_4)_2 \cdot 6H_2O$ in Ar at room temperature (Supporting Information Scheme S1).[40,45,46] Liquid chromatography mass spectrometry (LC-MS) of $[Co_2(OH)(L\text{-}Br)](ClO_4)_3$ shows two strong ion peaks at *m/z* 298.0 and 332.3, corresponding to the species of $\{[Co(L\text{-}Br)]^{2+} + H^+\}$ and $\{[Co_2(L\text{-}Br)]^{4+} + HCOO^-\}$, respectively (Supporting Information Figure S1). Then, $[Co_2(OH)(L\text{-}Br)](ClO_4)_3$ was dissolved in acetonitrile, followed by the slow diffusion of ethanol in air at room temperature to produce bottle-green crystals. Single-crystal X-ray structural analysis revealed that each asymmetric unit contained one $[Co_2(O_2COCH_2CH_3)(L\text{-}Br)]^{3+}$ cation and three ClO_4^- anions (Supporting Information Figure S2a and Table S1). This result suggests the occurrence of CO_2 fixation to form bicarbonate, and followed by esterification with ethanol to generate alkylcarbonate during the process of crystal growth (Supporting Information Scheme S1).[46] To confirm this, high-resolution MS (HR-MS) was performed. The results show two high-intensity ion peaks at *m/z* 347.7 and 571.0, corresponding to $[Co_2(O_2COCH_2CH_3)(L\text{-}Br)]^{3+}$ and $\{[Co_2(O_2COCH_2CH_3)(L\text{-}Br)](ClO_4)\}^{2+}$, respectively (Supporting Information Figures S3–S5). Moreover, the $[Co_2(O_2COCH_2CH_3)(L\text{-}Br)](ClO_4)_3$ asymmetric units were connected through hydrogen bond interactions to form a three-dimensional network (Supporting Information Figure S2b).

Subsequently, **Co_2-P_1** and **Co_2-P_2** were synthesized via a Sonogashira–Hagihara C–C coupling reaction between $[Co_2(OH)(L\text{-}Br)](ClO_4)_3$ and 1,4-diethynylbenzene/ 4,4′-diethynyl-1,1′-biphenyl (Figure 1). Fourier transform infrared spectroscopy (FTIR) profiles of **Co_2-P_1** and **Co_2-P_2** exhibited characteristic peaks at 2205 and 2208 cm^{-1}, respectively, corresponding to asymmetric alkyne bonds (-C≡C-). These results demonstrate the presence of alkynyl linkages in **Co_2-P_1** and **Co_2-P_2** (Figure 2a).[36,47,48] Raman spectra of **Co_2-P_1** and **Co_2-P_2** display the characteristic peaks at 2204 and 2207 cm^{-1}, respectively, also corresponding to the asymmetric alkyne bonds (–C≡C–),

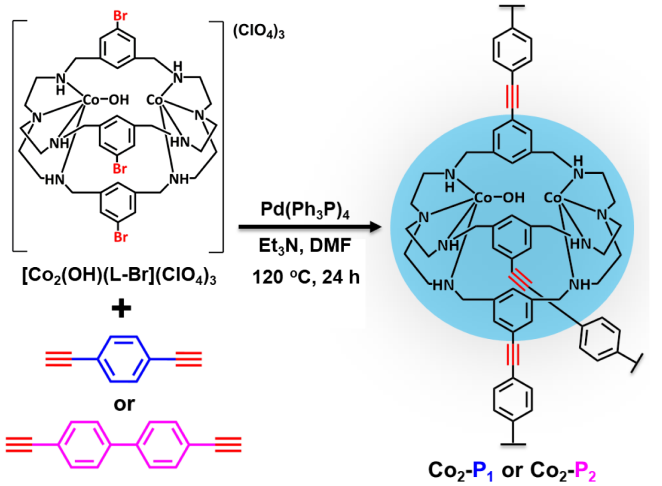

Figure 1 | *Schematic representation of the synthesis of* ***Co_2-P_1*** *and* ***Co_2-P_2*** *via Sonogashira–Hagihara C–C coupling reaction.*

further confirming the formation of alkynyl linkages (Figure 2b).[47,48] The powder X-ray diffraction patterns of both **Co_2-P_1** and **Co_2-P_2** show broad peaks at 2θ ≈ 22°, indicating the absence of long-range order and their amorphous nature (Supporting Information Figure S6). Scanning electron microscopy images of **Co_2-P_1** and **Co_2-P_2** showed a spherical morphology with a size of approximately 700 nm (Supporting Information Figure S7). Energy dispersive spectroscopy (EDS) mapping of **Co_2-P_1** and **Co_2-P_2** revealed a homogeneous distribution of C, N, O, Cl, and Co (Supporting Information Figures S8 and S9). The chemical compositions of **Co_2-P_1** and **Co_2-P_2** were further investigated by X-ray photoelectron spectroscopy (XPS). The XPS spectra showed the binding energies of C, N, O, Cl, and Co, which were consistent with the EDS results (Supporting Information Figures S10 and S11). The above results demonstrate the formation of cationic polymers of **Co_2-P_1** and **Co_2-P_2**, which are balanced by ClO_4^- anions. In addition, the inductively coupled plasma mass spectrometry (ICP-MS) analysis reveals that the Co contents for **Co_2-P_1** and **Co_2-P_2** are 9.70 and 8.37 wt % (Supporting Information Table S2), which are similar to the theoretical values of 9.68 and 8.85 wt %, respectively, that is, each dinuclear cobalt cryptate links three 1,4-diethynylbenzene or 4,4′-diethynyl-1,1′-biphenyl, as well as each 1,4-diethynylbenzene or 4,4′-diethynyl-1,1′-biphenyl connects two dinuclear cobalt cryptates to form **Co_2-P_1** or **Co_2-P_2** polymer.

The Co oxidation states of **Co_2-P_1** and **Co_2-P_2** were determined by XPS. The Co 2p XPS spectrum of **Co_2-P_1** displayed two characteristic peaks at 796.2 and 780.6 eV, corresponding to the binding energies of Co $2p_{1/2}$ and Co $2p_{3/2}$, respectively. Furthermore, two corresponding satellite peaks at 802.5 and 785.7 eV were also observed, demonstrating that the Co species in **Co_2-P_1** is +2

DOI: 10.31635/ccschem.024.202404675
Citation: *CCS Chem.* **2024**, 6, 3030–3040
Link to VoR: https://doi.org/10.31635/ccschem.024.202404675

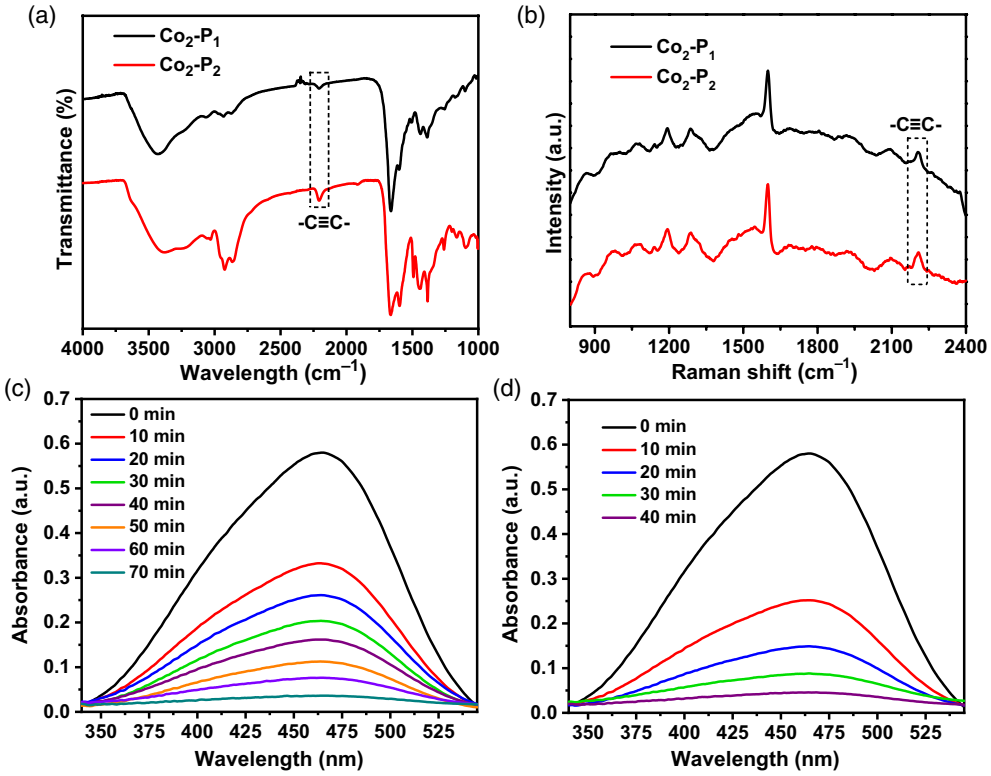

Figure 2 | *(a) FTIR spectra of* ***Co₂-P₁*** *and* ***Co₂-P₂****. (b) Raman spectra of* ***Co₂-P₁*** *and* ***Co₂-P₂****. UV–vis spectra of aqueous methyl orange solutions after soaking (c)* ***Co₂-P₁*** *and (d)* ***Co₂-P₂*** *at given intervals.*

oxidation state (Supporting Information Figure S12).[49,50] For **Co_2-P_2**, the binding energies of Co $2p_{1/2}$ and Co $2p_{3/2}$ were located at 796.5 and 780.8 eV, respectively, with two satellite peaks at 802.4 and 785.9 eV, also indicating the +2 oxidation state of Co species in **Co_2-P_2** (Supporting Information Figure S13).[49,50]

The porosity of **Co_2-P_1** and **Co_2-P_2** were examined by guest molecule adsorption experiments. First, the CO_2 adsorption isotherms show that the CO_2 adsorption capacities of **Co_2-P_1** and **Co_2-P_2** at 196 K and 1 atm are 63.7 and 73.9 $cm^3\ g^{-1}$ (standard temperature and pressure), respectively, which are higher than that of $[Co_2(OH)(L\text{-}Br)](ClO_4)_3$ (25.1 $cm^3\ g^{-1}$), revealing that the heterogenization of the molecular catalyst into porous polymers boosts the CO_2 adsorption capacity. The corresponding Brunauer–Emmett–Teller surface areas of **Co_2-P_1** and **Co_2-P_2** are 284 and 318 $m^2\ g^{-1}$, respectively (Supporting Information Figure S14). Moreover, the methyl orange adsorption experiment was conducted by soaking **Co_2-P_1** and **Co_2-P_2** in an aqueous solution of methyl orange. The adsorption of **Co_2-P_1** to methyl orange can be clearly observed by the change of solution color from faint yellow to colorless after 70 min (Supporting Information Figure S15). In contrast, the adsorption of **Co_2-P_2** to methyl orange was achieved within 40 min (Supporting Information Figure S16). Besides, the concentration of methyl orange was monitored by UV–vis spectroscopy at different time intervals. As shown in Figure 2c,d, the methyl orange adsorption peak at approximately 464 nm gradually decreases with increasing soaking time. This characteristic peak nearly disappeared after 70 min for **Co_2-P_1** and 40 min for **Co_2-P_2**. To further assess their porosity, I_2 adsorption experiments were carried out by soaking **Co_2-P_1** and **Co_2-P_2** in an *n*-hexane solution of I_2. Both **Co_2-P_1** and **Co_2-P_2** could adsorb I_2 by observing the change of I_2 adsorption peak in UV–vis spectroscopy at approximately 521 nm. As shown in Supporting Information Figure S17, I_2 concentration gradually decreased with increasing soaking time. The I_2 characteristic absorption peak nearly disappeared at 100 min for **Co_2-P_1**, whereas this phenomenon was observed at 80 min for **Co_2-P_2**. Similar phenomenon was observed for 4,4′,4″,4‴-(porphyrin-5,10,15,20-tetrayl)tetrabenzoate adsorption ($TCPP^{4-}$: 1.6 nm, Supporting Information Figures S18 and S19). These results suggest that the pore sizes of **Co_2-P_1** and **Co_2-P_2** are >1.6 nm, and **Co_2-P_2** has a larger pore size than **Co_2-P_1**. Moreover, the pore sizes of both polymers were larger than that of photosensitizer $[Ru(phen)_3]^{2+}$ (1.3 nm, Supporting Information Figure S20). Additionally, density functional theory calculations were performed to quantitatively evaluate the intermolecular interactions between $[Ru(phen)_3](PF_6)_2$ and the $[Co_2(OH)(L\text{-}C{\equiv}C\text{-}C_6H_6\text{-})](ClO_4)_3$ fragment of **Co_2-P_1/Co_2-P_2**.[51,52] As

DOI: 10.31635/ccschem.024.202404675
Citation: *CCS Chem.* **2024**, 6, 3030–3040
Link to VoR: https://doi.org/10.31635/ccschem.024.202404675

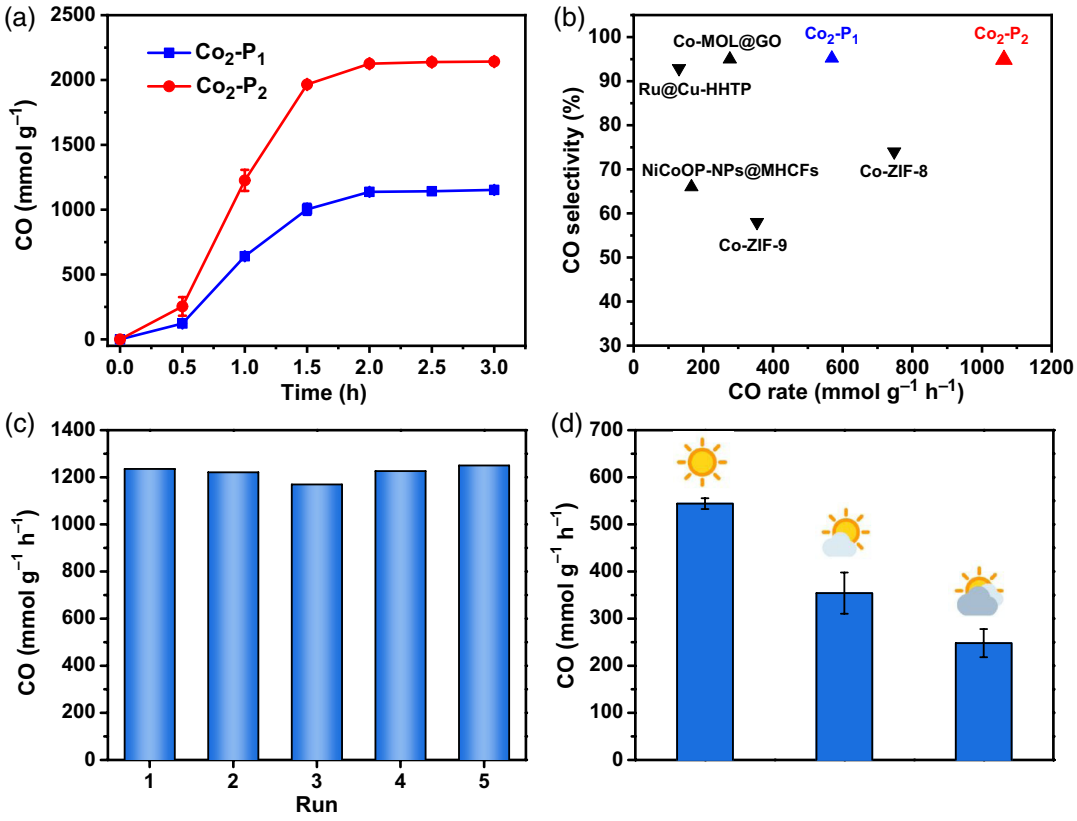

Figure 3 | *(a) CO yields of* ***Co₂-P₁*** *and* ***Co₂-P₂****. (b) Comparison of CO generation rate and selectivity over* ***Co₂-P₁*** *and* ***Co₂-P₂*** *with other reported heterogeneous catalysts. (c) Production rates of CO in five consecutive runs of photocatalytic CO_2 reduction over* ***Co₂-P₂*** *(2 h for each run). (d) Results of natural sunlight-driven CO_2 reduction over* ***Co₂-P₂*** *in 2 h.*

shown in Supporting Information Figure S21, the electrostatic force with an energy of −3118.26 kJ/mol dominates the total interactions, suggesting the strong affinity between $[Ru(phen)_3](PF_6)_2$ and **Co_2-P_1**/**Co_2-P_2**. The above results show that $[Ru(phen)_3](PF_6)_2$ can enter the pores of **Co_2-P_1**/**Co_2-P_2**, and **Co_2-P_2** could better encapsulate $[Ru(phen)_3]^{2+}$ to promote CO_2 photoreduction because of its larger pore size.

Photocatalytic CO_2 reduction experiments over **Co_2-P_1** and **Co_2-P_2** were performed in a CH_3CN/H_2O solution (v/v = 4:1) with $[Ru(phen)_3](PF_6)_2$ as the photosensitizer and BIH as the sacrificial electron donor. The gaseous products were analyzed via GC, and the liquid products were checked via ^1H nuclear magnetic resonance. The GC results demonstrate that the photocatalytic CO_2 reduction over **Co_2-P_1** and **Co_2-P_2** both generate a large amount of CO and a very small amount of H_2. As shown in Figure 3a, the CO yields for **Co_2-P_1** and **Co_2-P_2** increased rapidly in 2 h of visible-light irradiation with the CO generation rates of 568.8 and 1063.0 mmol g^{-1} h^{-1}, respectively. The turnover number (TON) values were 1391 and 2827 calculated with respect to per dinuclear cobalt cryptate, corresponding to TOF values of 11.6 and 23.6 min^{-1}, respectively (Supporting Information Figure S22 and Table S3). Obviously, by extending the linkers from phenyl in **Co_2-P_1** to biphenyl in **Co_2-P_2**, a higher catalytic efficiency for CO_2 photoreduction could be achieved. This result may be attributed to the larger pore size of **Co_2-P_2**, which could better accommodate $[Ru(phen)_3]^{2+}$ to promote electron transfer from the photosensitizer to the dinuclear cobalt center. Moreover, **Co_2-P_1** and **Co_2-P_2** display low H_2 production rates of 28.4 and 57.6 mmol g^{-1} h^{-1}, demonstrating that the photogenerated electrons primarily participate in the reduction of CO_2 to CO with selectivities of 95.2% and 94.9%, respectively (Supporting Information Figure S23). No products other than CO and H_2 were detected in the catalytic system (Supporting Information Figures S24 and S25).

Additionally, the photocatalytic CO_2 reduction experiment of the $[Co_2(OH)(L\text{-}Br)](ClO_4)_3$ molecular catalyst was conducted under the same conditions. After 2 h of light irradiation, the CO amount was 1.32 μmol, corresponding to TON and TOF values of 350 and 2.9 min^{-1}, respectively (Supporting Information Figure S26). Notably, **Co_2-P_2** shows larger TON and TOF values than those of $[Co_2(OH)(L\text{-}Br)](ClO_4)_3$ molecular catalyst, implying that the $[Ru(phen)_3]^{2+}$ encapsulated within the pore of

DOI: 10.31635/ccschem.024.202404675
Citation: *CCS Chem.* **2024**, 6, 3030–3040
Link to VoR: https://doi.org/10.31635/ccschem.024.202404675

Co_2-P_2 could better facilitate the electron transfer to the dinuclear cobalt center. To the best of our knowledge, **Co_2-P_2** displays the highest catalytic efficiency for photocatalytic CO_2 reduction among the heterogeneous catalysts reported so far, indicating that the heterogenization of molecular catalysts via a covalent strategy is an outstanding approach to obtaining high-efficiency catalysts for CO_2 photoreduction (Figure 3b and Supporting Information Table S3).[21-26,53,54]

Control experiments on **Co_2-P_2** were performed to confirm the carbon source of CO. The results show that negligible or even no CO was detected in the absence of **Co_2-P_2**, $[Ru(phen)_3](PF_6)_2$, BIH, CO_2, or light illumination (Supporting Information Table S4), indicating that these factors are indispensable for photocatalytic CO_2 reduction. Furthermore, a $^{13}CO_2$ isotope trace experiment was performed to validate the CO carbon source. As shown in Supporting Information Figure S27, the mass spectrum presents a signal peak at m/z = 29 attributed to ^{13}CO, verifying that the produced CO indeed originates from CO_2 reduction.[49] Previous reports have demonstrated that H_2O can act as a proton source for CO_2-to-CO conversion.[55-57] To confirm this, the photocatalytic CO_2 reduction experiment over **Co_2-P_2** in pure CH_3CN was conducted. A negligible amount of CO was detected in the absence of H_2O, suggesting that H_2O was an effective proton source for the reaction (Supporting Information Table S4, entry 7).

In addition to catalytic activity and selectivity, the durability of **Co_2-P_2** during CO_2 photoreduction was studied. As shown in Figure 3a, the CO yield remained unchanged after 2 h of light irradiation, which may be attributed to the degradation of $[Ru(phen)_3](PF_6)_2$, because it is prone to decompose under light irradiation.[40,42] To verify this, consecutive CO_2 photoreduction experiments were conducted. After 2 h of light irradiation, an equivalent of fresh $[Ru(phen)_3](PF_6)_2$ was added to the reaction system. It was observed that the ceased photocatalytic reaction could be reactivated at a similar CO production rate. With fresh $[Ru(phen)_3](PF_6)_2$ further added after 4 h, the ceased photocatalytic CO_2 reduction reaction could be reactivated again (Supporting Information Figure S28). These observations indicate that the cessation of CO_2 photoreduction after 2 and 4 h can be attributed to the consumption of $[Ru(phen)_3](PF_6)_2$, which in turn illustrates that **Co_2-P_2** is robust during the process of CO_2 photoreduction. Furthermore, the photocatalytic stability of **Co_2-P_2** was evaluated through recycling experiments. No discernible decrease in CO generation rate was observed during five consecutive cycles, indicative of the excellent stability of **Co_2-P_2** (Figure 3c). After the photocatalytic reaction, the FTIR and Raman spectra of **Co_2-P_2** still presented the characteristic peak of the asymmetrical alkyne bonds (–C≡C–) at approximately 2209 cm^{-1} (Supporting Information Figures S29 and S30). These results, together with the ICP-MS data showing that no Co^{2+} was leached in the solution after the CO_2 photoreduction, reveal that **Co_2-P_2** indeed has a high stability for the CO_2 photoreduction reaction. Furthermore, the XPS results demonstrated that the valence state of Co in **Co_2-P_2** remained unchanged during the photocatalytic reaction (Supporting Information Figure S31). In addition, the results of FTIR, Raman spectroscopy, and ICP-MS for **Co_2-P_1** also suggest its outstanding stability in the CO_2 photoreduction reaction (Supporting Information Figures S30 and S32). Besides, the apparent quantum yields of **Co_2-P_1** and **Co_2-P_2** determined at 450 nm were 0.23% and 0.46%, respectively.

Considering the extraordinary catalytic activity of **Co_2-P_2** for CO_2 photoreduction under a laboratory light source, we further tested the photocatalytic performance of **Co_2-P_2** under natural sunlight.[58,59] Solar-driven CO_2 reduction experiments were performed in a CH_3CN/H_2O solution (v/v = 4:1) with $[Ru(phen)_3](PF_6)_2$ as the photosensitizer and BIH as the sacrificial agent from 12:00 am to 2:00 pm. As shown in Figure 3d, **Co_2-P_2** also exhibits excellent catalytic activity under sunny days, with high CO production rate of 544.1 mmol g^{-1} h^{-1}, and large TON and TOF values of 1447 and 12.1 min^{-1}, respectively (with respect to per dinuclear cobalt cryptate). Moreover, the CO generation rates are 354.1 and 247.9 mmol g^{-1} h^{-1} under cloudy and overcast days, respectively. The CO selectivities of **Co_2-P_2** under the three weather conditions were 97.2%, 97.9%, and 98.4%, respectively. Such high catalytic performance for photochemical CO_2-to-CO conversion under natural sunlight has not yet been documented, to the best of our knowledge. These results provide solid evidence that **Co_2-P_2** displays exceptionally high catalytic performance for CO_2 photoreduction and further highlight the importance of the covalent strategy to construct heterogeneous catalysts for CO_2 photoreduction. For further comparison, similar amorphous polymers (**Co_2-P_3** and **Co_2-P_4**) were synthesized by the reaction of $[Co_2(OH)(L\text{-}Br)](ClO_4)_3$ with 1,3-diethynylbenzene and 4,4′′-diethynyl-1,1′:4′,1′′-terphenyl, respectively (Supporting Information Figures S33–S35 and Scheme S2). The results of the guest molecule adsorption experiments show that the pore size follows the order **Co_2-P_1** < **Co_2-P_3** < **Co_2-P_2** < **Co_2-P_4** (Figure 2c,d and Supporting Information Figures S36 and S37). For **Co_2-P_3** and **Co_2-P_4**, the Co contents are 9.33 and 8.07 wt %, respectively, and the Co oxidation states are +2 (Supporting Information Figures S38 and S39 and Table S2). The results of the photocatalytic CO_2 reduction demonstrate that the CO production rates of **Co_2-P_3** and **Co_2-P_4** are 790 and 1660 mmol g^{-1} h^{-1}, respectively. Therefore, the photocatalytic activities of all four polymers follow the same order **Co_2-P_1** < **Co_2-P_3** < **Co_2-P_2** < **Co_2-P_4**, further evidencing that a polymer with a larger pore size could

DOI: 10.31635/ccschem.024.202404675
Citation: *CCS Chem.* **2024**, 6, 3030–3040
Link to VoR: https://doi.org/10.31635/ccschem.024.202404675

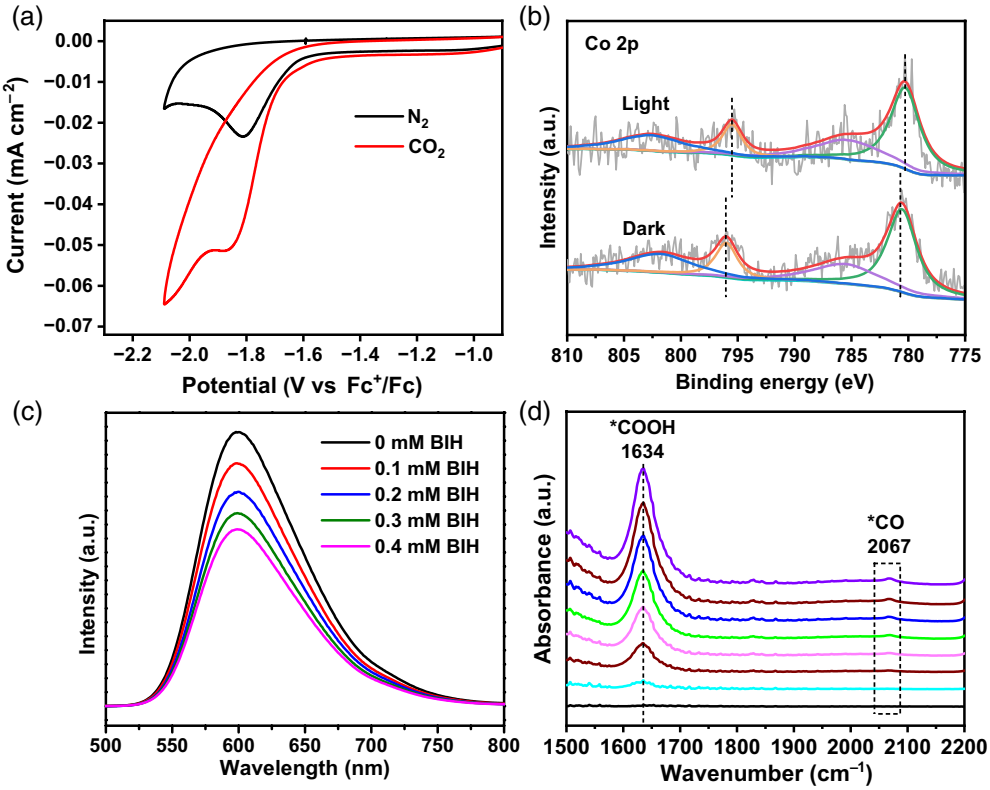

Figure 4 | *(a) CV curves of* ***Co$_2$-P$_2$*** *in CH_3CN/H_2O (v/v = 4:1) containing 0.1 M NBu_4PF_6 under N_2 or CO_2 atmospheres, respectively. (b) XPS spectra of Co 2p for* ***Co$_2$-P$_2$*** *in the dark and under light illumination. (c) PL spectra of $[Ru(phen)_3](PF_6)_2$ after addition of BIH at different concentrations (λ_{ex} = 420 nm). (d) In situ FTIR spectra of* ***Co$_2$-P$_2$*** *in the process of photocatalytic CO_2 reduction.*

better accommodate $[Ru(phen)_3]^{2+}$ to enhance catalytic performance (Supporting Information Figure S40).

A possible mechanism for the photocatalytic CO_2 reduction to CO with **Co$_2$-P$_2$** was investigated. The cyclic voltammogram (CV) of **Co$_2$-P$_2$** in N_2 atmosphere exhibits a primary reduction wave at –1.81 V versus Fc^+/Fc, which is due to the reduction of Co^{II} to Co^{I} (Figure 4a).[44] The CV of **Co$_2$-P$_2$** in CO_2 atmosphere shows a similar reduction wave at –1.87 V versus Fc^+/Fc, but with a significantly larger current, suggesting the occurrence of electrocatalysis (Figure 4a). Moreover, the XPS spectra of **Co$_2$-P$_2$** with $[Ru(phen)_3](PF_6)_2$ were recorded under dark and light-illumination conditions. In the dark, **Co$_2$-P$_2$** shows two characteristic peaks at 796.0 and 780.7 eV in Co 2p spectrum, corresponding to the binding energies of Co $2p_{1/2}$ and Co $2p_{3/2}$, respectively (Figure 4b). Upon light illumination, the binding energies of Co $2p_{1/2}$ and Co $2p_{3/2}$ shift to 795.5 and 780.3 eV, respectively, suggesting that Co^{II} accepts an electron from the excited $[Ru(phen)_3]^{2+*}$, and thus converts to Co^{I} (Figure 4b). Additionally, fluorescence quenching experiments on $[Ru(phen)_3]^{2+}$ with different amounts of BIH or **Co$_2$-P$_2$** were carried out. As shown in Figure 4c, the fluorescence emission peak of $[Ru(phen)_3]^{2+*}$ was located at 599 nm under an excitation wavelength of 450 nm, which was gradually quenched with increasing concentrations of BIH. The quenching rate constant (k_q) was 4.80 × 10^9 M^{-1} s^{-1}, as evaluated by Stern-Volmer plots (Supporting Information Figure S41). In stark contrast, negligible fluorescence changes in the excited $[Ru(phen)_3]^{2+*}$ were observed upon the addition of varying concentrations of **Co$_2$-P$_2$** (Supporting Information Figures S42 and S43). These results demonstrate that the excited $[Ru(phen)_3]^{2+*}$ follows a reductively quenching mechanism.[42,60] Thus, upon illumination, $[Ru(phen)_3]^{2+}$ is excited to produce the excited $[Ru(phen)_3]^{2+*}$, which transfers an electron to the Co^{II} of **Co$_2$-P$_2$** to generate Co^{I}. This result is in good agreement with the XPS analysis above (Figure 4b). The generated Co^{I} further reduces the adsorbed CO_2 to CO. To monitor the key intermediates in the photoreduction of CO_2 to CO, in situ FTIR measurements over **Co$_2$-P$_2$** were conducted. As shown in Figure 4d, two new absorption peaks were observed at 1634 and 2067 cm^{-1}, and their intensities gradually increased with increasing illumination time. They can be assigned to the *COOH and *CO intermediates respectively, which are the key intermediates in photocatalytic CO_2 reduction to CO.[61,62]

In order to elucidate the higher catalytic performance for CO_2 photoreduction of **Co$_2$-P$_2$** than **Co$_2$-P$_1$**,

DOI: 10.31635/ccschem.024.202404675
Citation: *CCS Chem.* **2024**, 6, 3030–3040
Link to VoR: https://doi.org/10.31635/ccschem.024.202404675

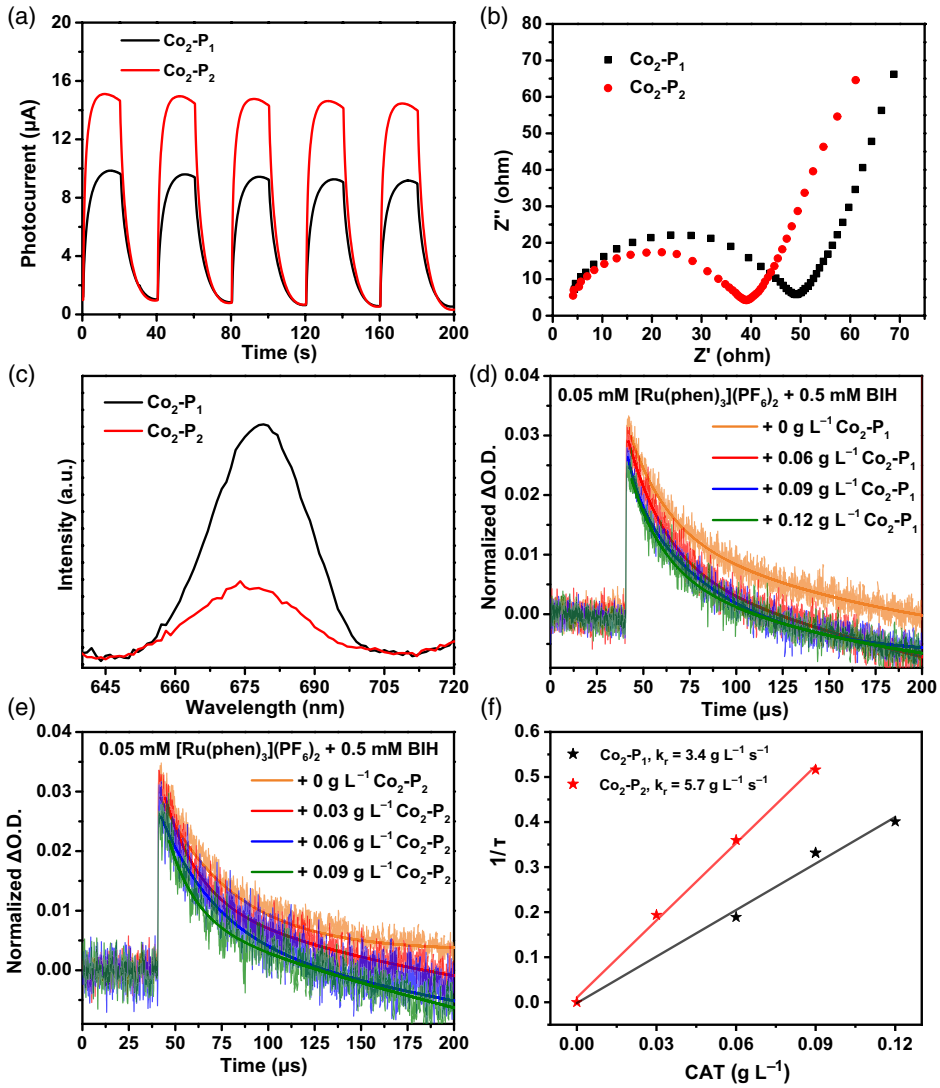

Figure 5 | *(a) Photocurrent tests for* ***Co₂-P₁*** *and* ***Co₂-P₂****. (b) EIS plots of* ***Co₂-P₁*** *and* ***Co₂-P₂****. (c) PL spectra of* ***Co₂-P₁*** *and* ***Co₂-P₂*** *under excitation at 450 nm. (d) Kinetic traces of 0.05 mM [Ru(phen)₃](PF₆)₂ with 0.5 mM BIH and 0–0.12 g L⁻¹* ***Co₂-P₁****. (e) Kinetic traces of 0.05 mM [Ru(phen)₃](PF₆)₂ with 0.5 mM BIH and 0–0.09 g L⁻¹* ***Co₂-P₂****. (f) Plot of 1/τ versus the concentrations of* ***Co₂-P₁*** *and* ***Co₂-P₂*** *with linear fitting for the [Ru(phen)₃](PF₆)₂ system with BIH.*

photocurrent, electrochemical impedance spectroscopy (EIS), and photoluminescence (PL) measurements of **Co_2-P_1** and **Co_2-P_2** were performed.[63,64] The results demonstrate that **Co_2-P_2** exhibits a higher photocurrent response than **Co_2-P_1**, indicating that it has faster electron transfer (Figure 5a). The EIS results showed that **Co_2-P_2** had a smaller semicircle radius, indicative of its lower charge-transfer resistance (Figure 5b). Furthermore, the PL spectra show that the emission intensity of **Co_2-P_2** is weaker than that of **Co_2-P_1**, implying the faster electron transfer for **Co_2-P_2** than **Co_2-P_1** (Figure 5c). The above results show that the extension of linkers from phenyl in **Co_2-P_1** to biphenyl in **Co_2-P_2** significantly facilitates electron transfer from $[Ru(phen)_3](PF_6)_2$ to the Co catalytic sites, thus accounting for the higher photocatalytic performance of **Co_2-P_2**. To further confirm the fast electron transfer, transient absorption spectra were recorded.[65,66] First, a strong bleaching band at around 440 nm and a positive absorption band at approximately 502 nm for $[Ru(phen)_3]^{2+}$ were observed upon pulsed laser excitation at 440 nm, which can be attributed to metal-to-ligand charge transfer (Supporting Information Figure S44). After addition of 0.5 mM BIH, the positive absorption band was obviously strengthened, implying the formation of reduced $[Ru(phen)_3]^{2+}$, further supporting the reductive quenching pathway (Supporting Information Figure S45). Subsequently, different concentrations of **Co_2-P_1** or **Co_2-P_2** were added to the mixed solution. As shown in Figure 5d,e, the lifetime of the reduced-state species decreases along with the enhanced concentrations of **Co_2-P_1** or **Co_2-P_2**. The second-order reaction constant (k_r) of reduced $[Ru(phen)_3]^{2+}$ were

DOI: 10.31635/ccschem.024.202404675
Citation: *CCS Chem.* **2024**, 6, 3030–3040
Link to VoR: https://doi.org/10.31635/ccschem.024.202404675

determined as 3.4 L g^{-1} s^{-1} by **Co_2-P_1** and 5.7 L $g^{-1}s^{-1}$ by **Co_2-P_2**, suggesting the faster electron transfer rate from $[Ru(phen)_3](PF_6)_2$ to **Co_2-P_2** than **Co_2-P_1** (Figure 5f). Therefore, the photoreduction of Co^{II} to Co^{I} species in **Co_2-P_2** proceeds more easily than that in **Co_2-P_1** in the process of CO_2 reduction, further explaining the higher photocatalytic performance of **Co_2-P_2** than tha of **Co_2-P_1**.

Conclusion

In summary, by covalently linking a dinuclear cobalt complex with phenyl/biphenyl linkers, we developed two high-performance polymers (**Co_2-P_1** and **Co_2-P_2**) for photocatalytic CO_2 reduction. Remarkably, **Co_2-P_2** with a biphenyl linker exhibited faster electron transfer from the photosensitizer to the catalyst than **Co_2-P_1** with a phenyl linker. Consequently, **Co_2-P_2** not only exhibits higher catalytic performance for photochemical CO_2-to-CO conversion than **Co_2-P_1**, but also achieves the record-high CO generation rate of 1063.0 mmol g^{-1} h^{-1} and TOF value of 23.6 min^{-1} under a laboratory light source among all reported heterogeneous catalysts. Additionally, **Co_2-P_2** also displays an impressive catalytic activity for CO_2 photoreduction under natural sunlight with CO generation rate of 544.1 mmol g^{-1} h^{-1} and TOF value of 12.1 min^{-1}. This study paves the way for the development of highly active catalysts for CO_2 photoreduction.

Supporting Information

Supporting Information is available and includes detailed experimental procedures, characterizations, Schemes S1 and S2, additional Figures S1–S45, and Tables S1–S4.

Conflict of Interest

There is no conflict of interest to report.

Funding Information

This work was supported by National Key R&D Program of China (grant no. 2022YFA1502902), the National Natural Science Foundation of China (grant nos. 22371208, 22271218, 22071182, and 21931007), and the Science & Technology Development Fund of Tianjin Education Commission for Higher Education (grant no. 2018KJ129).

References

1. Ding, M.; Flaig, R. W.; Jiang, H.-L.; Yaghi, O. M. Carbon Capture and Conversion Using Metal-Organic Frameworks and MOF-Based Materials. *Chem. Soc. Rev.* **2019**, *48*, 2783–28281.
2. Wu, Q.-J.; Liang, J.; Huang, Y.-B.; Cao, R. Thermo-, Electro-, and Photocatalytic CO_2 Conversion to Value-Added Products over Porous Metal/Covalent Organic Frameworks. *Acc. Chem. Res.* **2022**, *55*, 2978–2997.
3. Wang, C.; Lv, Z.; Yang, W.; Feng, X.; Wang, B. A Rational Design of Functional Porous Frameworks for Electrocatalytic CO_2 Reduction Reaction. *Chem. Soc. Rev.* **2023**, *52*, 1382–1427.
4. Wang, Z.; Yang, Z.; Kadirova, Z. C.; Guo, M.; Fang, R.; He, J.; Yan, Y.; Ran, J. Photothermal Functional Material and Structure for Photothermal Catalytic CO_2 Reduction: Recent Advance, Application and Prospect. *Coord. Chem. Rev.* **2022**, *473*, 214794.
5. Jiang, Z.; Xu, X.; Ma, Y.; Cho, H. S.; Ding, D.; Wang, C.; Wu, J.; Oleynikov, P.; Jia, M.; Cheng, J.; Zhou, Y.; Terasaki, O.; Peng, T.; Zan, L.; Deng, H. Filling Metal-Organic Framework Mesopores with TiO_2 for CO_2 Photoreduction. *Nature* **2020**, *586*, 549–554.
6. Kong, T.; Jiang, Y.; Xiong, Y. Photocatalytic CO_2 Conversion: What Can We Learn from Conventional CO_x Hydrogenation? *Chem. Soc. Rev.* **2020**, *49*, 6579–6591.
7. Yoshino, S.; Takayama, T.; Yamaguchi, Y.; Iwase, A.; Kudo, A. CO_2 Reduction Using Water as an Electron Donor over Heterogeneous Photocatalysts Aiming at Artificial Photosynthesis. *Acc. Chem. Res.* **2022**, *55*, 966–977.
8. Li, J.; Huang, H.; Xue, W.; Sun, K.; Song, X.; Wu, C.; Nie, L.; Li, Y.; Liu, C.; Pan, Y.; Jiang, H.-L.; Mei, D.; Zhong, C. Self-Adaptive Dual-Metal-Site Pairs in Metal-Organic Frameworks for Selective CO_2 Photoreduction to CH_4. *Nat. Catal.* **2021**, *4*, 719–729.
9. Luo, T.; Wang, Z.; Han, X.; Chen, Y.; Iuga, D.; Lee, D.; An, B.; Xu, S.; Kang, X.; Tuna, F.; McInnes, E. J. L.; Hughes, L.; Spencer, B. F.; Schröder, M.; Yang, S. Efficient Photocatalytic Reduction of CO_2 Catalyzed by the Metal-Organic Framework MFM-300(Ga). *CCS Chem.* **2022**, *4*, 2560–2569.
10. Zhang, L.; Li, R.-H.; Li, X.-X.; Liu, J.; Guan, W.; Dong, L.-Z.; Li, S.-L.; Lan, Y.-Q. Molecular Oxidation-Reduction Junctions for Artificial Photosynthetic Overall Reaction. *Proc. Natl. Acad. Sci. U. S. A.* **2022**, *119*, e2210550119.
11. Chen, L.; Chen, G.; Leung, C.-F.; Cometto, C.; Robert, M.; Lau, T.-C. Molecular Quaterpyridine-Based Metal Complexes for Small Molecule Activation: Water Splitting and CO_2 Reduction. *Chem. Soc. Rev.* **2020**, *49*, 7271–7283.
12. Wang, J.-W.; Liu, W.-J.; Zhong, D.-C.; Lu, T.-B. Nickel Complexes as Molecular Catalysts for Water Splitting and CO_2 Reduction. *Coord. Chem. Rev.* **2019**, *378*, 237–261.
13. Hong, D.; Kawanishi, T.; Tsukakoshi, Y.; Kotani, H.; Ishizuka, T.; Kojima, T. Efficient Photocatalytic CO_2 Reduction by a Ni(II) Complex Having Pyridine Pendants Through Capturing a Mg^{2+} Ion as a Lewis-Acid Cocatalyst. *J. Am. Chem. Soc.* **2019**, *141*, 20309–20317.
14. Wei, Y.; Li, J.; Zhao, D.; Zhao, Y.; Zhang, Q.; Gu, L.; Wan, J.; Wang, D. ZnO HoMS@ZIF-8 Nanoreactors for Efficient Enrichment and Photoreduction of Atmospheric CO_2. *CCS Chem.* **2024**. DOI: https://doi.org/10.31635/ccschem.024.202303604
15. Sun, K.; Qian, Y.; Jiang, H.-L. Metal-Organic Frameworks for Photocatalytic Water Splitting and CO_2 Reduction. *Angew. Chem. Int. Ed.* **2023**, *62*, e202217565.

DOI: 10.31635/ccschem.024.202404675
Citation: *CCS Chem.* **2024**, 6, 3030–3040
Link to VoR: https://doi.org/10.31635/ccschem.024.202404675

16. Wang, X.; He, J.; Chen, X.; Ma, B.; Zhu, M. Metal Halide Perovskites for Photocatalytic CO_2 Reduction: An Overview and Prospects. *Coord. Chem. Rev.* **2023**, *482*, 215076.
17. Ji, S.; Qu, Y.; Wang, T.; Chen, Y.; Wang, G.; Li, X.; Dong, J.; Chen, Q. Y.; Zhang, W.; Zhang, Z.; Liang, S.; Yu, R.; Wang, Y.; Wang, D.; Li, Y. Rare-Earth Single Erbium Atoms for Enhanced Photocatalytic CO_2 Reduction. *Angew. Chem. Int. Ed.* **2020**, *59*, 10651–10657.
18. Li, W.; Elzatahry, A.; Aldhayan, D.; Zhao, D. Core-Shell Structured Titanium Dioxide Nanomaterials for Solar Energy Utilization. *Chem. Soc. Rev.* **2018**, *47*, 8203–8237.
19. Zhang, L.; Liu, J.; Lan, Y.-Q. Hetero-Motif Molecular Junction Photocatalysts: A New Frontier in Artificial Photosynthesis. *Acc. Chem. Res.* **2024**, *57*, 870–883.
20. Verma, P.; Rahimi, F. A.; Samanta, D.; Kundu, A.; Dasgupta, J.; Maji, T. K. Visible-Light-Driven Photocatalytic CO_2 Reduction to CO/CH_4 Using a Metal-Organic "Soft" Coordination Polymer Gel. *Angew. Chem. Int. Ed.* **2022**, *61*, e202116094.
21. Wang, J.-W.; Qiao, L.-Z.; Nie, H.-D.; Huang, H.-H.; Li, Y.; Yao, S.; Liu, M.; Zhang, Z.-M.; Kang, Z.-H.; Lu, T.-B. Facile Electron Delivery from Graphene Template to Ultrathin Metal-Organic Layers for Boosting CO_2 Photoreduction. *Nat. Commun.* **2021**, *12*, 813.
22. Wang, S.; Yao, W.; Lin, J.; Ding, Z.; Wang, X. Cobalt Imidazolate Metal-Organic Frameworks Photosplit CO_2 Under Mild Reaction Conditions. *Angew. Chem. Int. Ed.* **2014**, *53*, 1034–1038.
23. Huang, N.-Y.; He, H.; Liu, S. J.; Zhu, H.-L.; Li, Y.-J.; Xu, J.; Huang, J.-R.; Wang, X.; Liao, P.-Q.; Chen, X.-M. Electrostatic Attraction-Driven Assembly of a Metal-Organic Framework with a Photosensitizer Boosts Photocatalytic CO_2 Reduction to CO. *J. Am. Chem. Soc.* **2021**, *143*, 17424–17430.
24. Wang, Y.; Wang, S.; Lou, X. W. Dispersed Nickel Cobalt Oxyphosphide Nanoparticles Confined in Multichannel Hollow Carbon Fibers for Photocatalytic CO_2 Reduction. *Angew. Chem. Int. Ed.* **2019**, *58*, 17236–17240.
25. Rodríguez-Jiménez, S.; Song, H.; Lam, E.; Wright, D.; Pannwitz, A.; Bonke, S. A.; Baumberg, J. J.; Bonnet, S.; Hammarström, L.; Reisner, E. Self-Assembled Liposomes Enhance Electron Transfer for Efficient Photocatalytic CO_2 Reduction. *J. Am. Chem. Soc.* **2022**, *144*, 9399–9412.
26. Wei, Y.; Chen, L.; Chen, H.; Cai, L.; Tan, G.; Qiu, Y.; Xiang, Q.; Chen, G.; Lau, T.-C.; Robert, M. Highly Efficient Photocatalytic Reduction of CO_2 to CO by In Situ Formation of a Hybrid Catalytic System Based on Molecular Iron Quaterpyridine Covalently Linked to Carbon Nitride. *Angew. Chem. Int. Ed.* **2022**, *61*, e202116832.
27. Feng, X.; Pi, Y.; Song, Y.; Brzezinski, C.; Xu, Z.; Li, Z.; Lin, W. Metal-Organic Frameworks Significantly Enhance Photocatalytic Hydrogen Evolution and CO_2 Reduction with Earth-Abundant Copper Photosensitizers. *J. Am. Chem. Soc.* **2020**, *142*, 690–695.
28. Yan, Z.-H.; Ma,B.; Li, S.-R.; Liu, J.; Chen, R.; Du, M.-H.; Jin, S.; Zhuang, G.-L.; Long, L.-S.; Kong, X.-J.; Zheng, L.-S. Encapsulating a Ni(II) Molecular Catalyst in Photoactive Metal-Organic Framework for Highly Efficient Photoreduction of CO_2. *Sci. Bull.* **2019**, *64*, 976–985.
29. Fu, Z.; Shu, C.; Wang, X.; Chen, L.; Wang, X.; Liu, L.; Wang, K.; Clowes, R.; Chong, S. Y.; Wu, X.; Cooper, A. I. Fluorinated Covalent Organic Frameworks Coupled with Molecular Cobalt Cocatalysts for Efficient Photocatalytic CO_2 Reduction. *CCS Chem.* **2023**, *5*, 2290–2300.
30. Ma, B.; Chen, G.; Fave, C.; Chen, L.; Kuriki, R.; Maeda, K.; Ishitani, O.; Lau, T.-C.; Bonin, J.; Robert, M. Efficient Visible-Light-Driven CO_2 Reduction by a Cobalt Molecular Catalyst Covalently Linked to Mesoporous Carbon Nitride. *J. Am. Chem. Soc.* **2020**, *142*, 6188–6195.
31. Yang, W.; Wang, H.-J.; Liu, R.-R.; Wang, J.-W.; Zhang, C.; Li, C.; Zhong, D.-C.; Lu, T.-B. Tailoring Crystal Facets of Metal–Organic Layers to Enhance Photocatalytic Activity for CO_2 Reduction. *Angew. Chem. Int. Ed.* **2021**, *60*, 409–414.
32. Yu, B.; Meng, T.; Ding, X.; Liu, X.; Wang, H.; Chen, B.; Zheng, T.; Li, W.; Zeng, Q.; Jiang, J. Hydrogen-Bonded Organic Framework Ultrathin Nanosheets for Efficient Visible-Light Photocatalytic CO_2 Reduction. *Angew. Chem. Int. Ed.* **2022**, *61*, e202211482.
33. Lu, K.-Q.; Li, Y.-H.; Zhang, F.; Qi, M.-Y.; Chen, X.; Tang, Z.-R.; Yamada, Y. M. A.; Anpo, M.; Conte, M.; Xu, Y.-J. Rationally Designed Transition Metal Hydroxide Nanosheet Arrays on Graphene for Artificial CO_2 Reduction. *Nat. Commun.* **2020**, *11*, 5181.
34. Dong, X.-Y.; Si, Y.-N.; Wang, Q.-Y.; Wang, S.; Zang, S.-Q. Integrating Single Atoms with Different Microenvironments into One Porous Organic Polymer for Efficient Photocatalytic CO_2 Reduction. *Adv. Mater.* **2021**, *33*, 2101568.
35. Zhou, W.; Deng, Q.-W.; He, H.-J.; Yang, L.; Liu, T.-Y.; Wang, X.; Zheng, D.-Y.; Dai, Z.-B.; Sun, L.; Liu, C.; Wu, H.; Li, Z.; Deng, W.-Q. Heterogenization of Salen Metal Molecular Catalysts in Covalent Organic Frameworks for Photocatalytic Hydrogen Evolution. *Angew. Chem. Int. Ed.* **2023**, *62*, e202214143.
36. Barman, S.; Singh, A.; Rahimi, F. A.; Maji, T. K. Metal-Free Catalysis: A Redox-Active Donor-Acceptor Conjugated Microporous Polymer for Selective Visible-Light-Driven CO_2 Reduction to CH_4. *J. Am. Chem. Soc.* **2021**, *143*, 16284–16292.
37. Huang, Q.; Niu, Q.; Li, X.-F.; Liu, J.; Sun, S.-N.; Dong, L.-Z.; Li, S.-L.; Cai, Y.-P.; Lan, Y.-Q. Demystifying the Roles of Single Metal Site and Cluster in CO_2 Reduction via Light and Electric Dual-Responsive Polyoxometalate-Based Metal-Organic Frameworks. *Sci. Adv.* **2022**, *8*, eadd5598.
38. Zhang, J.-H.; Gong, Y.-N.; Wang, H.-J.; Wang, Y.-C.; Yang, W.; Mei, J.-H.; Zhong, D.-C.; Lu, T.-B. Ordered Heterogeneity of Molecular Photosensitizer Toward Enhanced Photocatalysis. *Proc. Natl. Acad. Sci.* **2022**, *119*, e2118278119.
39. Zhu, H.-L.; Chen, H.-Y.; Han, Y.-X.; Zhao, Z.-H.; Liao, P.-Q.; Chen, X.-M. A Porous π-π Stacking Framework with Dicopper(I) Sites and Adjacent Proton Relays for Electroreduction of CO_2 to C_{2+} Products. *J. Am. Chem. Soc.* **2022**, *144*, 13319–13326.
40. Ouyang, T.; Huang, H.-H.; Wang, J.-W.; Zhong, D.-C.; Lu, T.-B. A Dinuclear Cobalt Cryptate as a Homogeneous Photocatalyst for Highly Selective and Efficient Visible-Light Driven CO_2 Reduction to CO in CH_3CN/H_2O Solution. *Angew. Chem. Int. Ed.* **2017**, *56*, 738–743.
41. Guo, Z.; Chen, G.; Cometto, C.; Ma, B.; Zhao, H.; Groizard, T.; Chen, L.; Fan, H.; Man, W.-L.; Yiu, S.-M.; Lau, K.-C.; Lau, T.-C.; Robert, M. Selectivity Control of CO Versus $HCOO^-$ Production

DOI: 10.31635/ccschem.024.202404675
Citation: *CCS Chem.* **2024**, 6, 3030–3040
Link to VoR: https://doi.org/10.31635/ccschem.024.202404675

in the Visible-Light-Driven Catalytic Reduction of CO_2 with Two Cooperative Metal Sites. *Nat. Catal.* **2019**, *2*, 801–808.
42. Ouyang, T.; Wang, H.-J.; Huang, H.-H.; Wang, J.-W.; Guo, S.; Liu, W.-J.; Zhong, D.-C.; Lu, T.-B. Dinuclear Metal Synergistic Catalysis Boosts Photochemical CO_2-to-CO Conversion. *Angew. Chem. Int. Ed.* **2018**, *57*, 16480–16485.
43. Cao, L.-M.; Huang, H.-H.; Wang, J.-W.; Zhong, D.-C.; Lu, T.-B. The Synergistic Catalysis Effect Within a Dinuclear Nickel Complex for Efficient and Selective Electrocatalytic Reduction of CO_2 to CO. *Green Chem.* **2018**, *20*, 798–803.
44. Zhang, X.; Cibian, M.; Call, A.; Yamauchi, K.; Sakai, K. Photochemical CO_2 Reduction Driven by Water-Soluble Copper(I) Photosensitizer with the Catalysis Accelerated by Multi-Electron Chargeable Cobalt Porphyrin. *ACS Catal.* **2019**, *9*, 11263–11273.
45. Realista, S.; Almeida, J. C.; Milheiro, S. A.; Bandeira, N. A. G.; Alves, L. G.; Madeira, F.; Calhorda, M. J.; Martinho, P. N. CoII Cryptates Convert CO_2 into CO and CH_4 Under Visible Light. *Chem. Eur. J.* **2019**, *2*, 11670–11679.
46. Chen, J.-M.; Wei, W.; Feng, X.-L.; Lu, T.-B. CO_2 Fixation and Transformation by a Dinuclear Copper Cryptate Under Acidic Conditions. *Chem. Asian J.* **2007**, *2*, 710–719.
47. Zhou, W.; Shen, H.; Zeng, Y.; Yi, Y.; Zuo, Z.; Li, Y.; Li, Y. Controllable Synthesis of Graphdiyne Nanoribbons. *Angew. Chem. Int. Ed.* **2020**, *59*, 4908–4913.
48. Li, J.; Gao, X.; Liu, B.; Feng, Q.; Li, X.-B.; Huang, M.-Y.; Liu, Z.; Zhang, J.; Tung, C.-H.; Wu, L.-Z. Graphdiyne: A Metal-Free Material as Hole Transfer Layer to Fabricate Quantum Dot-Sensitized Photocathodes for Hydrogen Production. *J. Am. Chem. Soc.* **2016**, *138*, 3954–3957.
49. Gong, Y.-N.; Zhong, W.; Li, Y.; Qiu, Y.; Zheng, L.; Jiang, J.; Jiang, H.-L. Regulating Photocatalysis by Spin-State Manipulation of Cobalt in Covalent Organic Frameworks. *J. Am. Chem. Soc.* **2020**, *142*, 16723–16731.
50. Zhang, H.; Wei, J.; Dong, J.; Liu, G.; Shi, L.; An, P.; Zhao, G.; Kong, J.; Wang, X.; Meng, X.; Zhang, J.; Ye, J. Efficient Visible-Light-Driven Carbon Dioxide Reduction by a Single-Atom Implanted Metal-Organic Framework. *Angew. Chem. Int. Ed.* **2016**, *55*, 14310–14314.
51. Coppens, P.; Abramov, Y.; Carducci, M.; Korjov, B.; Novozhilova, I.; Alhambra, C.; Pressprich, M. R. Experimental Charge Densities and Intermolecular Interactions: Electrostatic and Topological Analysis of DL-Histidine. *J. Am. Chem. Soc.* **1999**, *121*, 2585–2593.
52. Cai, X.; Ding, D.; Zhao, S.; Wen, S.; Zhang, G.; Bai, P.; Zhang, W.; Song, H.; Xu, C. Zwitterionic Aqua Palladacycles with Noncovalent Interactions for Meta-Selective Suzuki Coupling of 3,4-Dichlorophenol and 3,4-Dichlorobenzyl Alcohol in Water. *Inorg. Chem.* **2024**, *63*, 2313–2321.
53. An, L.; Torre, P. D. L.; Smith, P. T.; Narouz, M. R.; Chang, C. J. Synergistic Porosity and Charge Effects in a Supramolecular Porphyrin Cage Promote Efficient Photocatalytic CO_2 Reduction. *Angew. Chem. Int. Ed.* **2023**, *62*, e202209396.
54. Arcudi, F.; Đorđevic, L.; Nagasing, B.; Stupp, S. I.; Weiss, E. A. Quantum Dot-Sensitized Photoreduction of CO_2 in Water with Turnover Number > 80,000. *J. Am. Chem. Soc.* **2021**, *143*, 18131–18138.
55. Yoshino, S.; Iwase, A.; Yamaguchi, Y.; Suzuki, T. M.; Morikawa, T.; Kudo, A. Photocatalytic CO_2 Reduction Using Water as an Electron Donor Under Visible Light Irradiation by Z-Scheme and Photoelectrochemical Systems over $(CuGa)_{0.5}ZnS_2$ in the Presence of Basic Additives. *J. Am. Chem. Soc.* **2022**, *144*, 2323–2332.
56. Huang, N.; Lee, K. H.; Yue, Y.; Xu, X.; Irle, S.; Jiang, Q.; Jiang, D. A Stable and Conductive Metallophthalocyanine Framework for Electrocatalytic Carbon Dioxide Reduction in Water. *Angew. Chem. Int. Ed.* **2020**, *59*, 16587–16593.
57. Wang, S.; Xu, M.; Peng, T.; Zhang, C.; Li, T.; Hussain, I.; Wang, J.; Tan, B. Porous Hypercrosslinked Polymer-TiO_2-Graphene Composite Photocatalysts for Visible-Light-Driven CO_2 Conversion. *Nat. Commun.* **2019**, *10*, 676.
58. Gao, S.; Zhang, Q.; Su, X.; Wu, X.; Zhang, X.-G.; Guo, Y.; Li, Z.; Wei, J.; Wang, H.; Zhang, S.; Wang, J. Ingenious Artificial Leaf Based on Covalent Organic Framework Membranes for Boosting CO_2 Photoreduction. *J. Am. Chem. Soc.* **2023**, *145*, 9520–9529.
59. Karmakar, S.; Barman, S.; Rahimi, F. A.; Maji, T. K. Covalent Grafting of Molecular Photosensitizer and Catalyst on MOF-808: Effect of Pore Confinement Toward Visible Light-Driven CO_2 Reduction in Water. *Energy Environ. Sci.* **2021**, *14*, 2429–2440.
60. Han, B.; Ou, X.; Deng, Z.; Song, Y.; Tian, C.; Deng, H.; Xu, Y.-J.; Lin, Z. Nickel Metal-Organic Framework Monolayers for Photoreduction of Diluted CO_2: Metal-Node-Dependent Activity and Selectivity. *Angew. Chem. Int. Ed.* **2018**, *57*, 16811–16815.
61. Li, X.; Sun, Y.; Xu, J.; Shao, Y.; Wu, J.; Xu, X.; Pan, Y.; Ju, H.; Zhu, J.; Xie, Y. Selective Visible-Light-Driven Photocatalytic CO_2 Reduction to CH_4 Mediated by Atomically Thin $CuIn_5S_8$ Layers. *Nat. Energy* **2019**, *4*, 690–699.
62. Li, Y.; Wei, B.; Zhu, M.; Chen, J.; Jiang, Q.; Yang, B.; Hou, Y.; Lei, L.; Li, Z.; Zhang, R.; Lu, Y. Synergistic Effect of Atomically Dispersed Ni-Zn Pair Sites for Enhanced CO_2 Electroreduction. *Adv. Mater.* **2021**, *33*, 2102212.
63. Qian, Y.; Han, Y.; Zhang, X.; Yang, G.; Zhang, G.; Jiang, H.-L. Computation-Based Regulation of Excitonic Effects in Donor-Acceptor Covalent Organic Frameworks for Enhanced Photocatalysis. *Nat. Commun.* **2023**, *14*, 3083.
64. Lu, M.; Zhang, M.; Liu, J.; Yu, T.-Y.; Chang, J.-N.; Shang, L.-J.; Li, S.-L.; Lan, Y.-Q. Confining and Highly Dispersing Single Polyoxometalate Clusters in Covalent Organic Frameworks by Covalent Linkages for CO_2 Photoreduction. *J. Am. Chem. Soc.* **2022**, *144*, 1861–1871.
65. Wang, J.-W.; Li, Z.; Luo, Z.-M.; Huang, Y.; Ma, F.; Kupfer, S.; Ouyang, G. Boosting CO_2 Photoreduction by π–π-Induced Preassembly Between a Cu(I) Sensitizer and a Pyrene-Appended Co(II) Catalyst. *Proc. Natl. Acad. Sci.* **2023**, *120*, e2221219120.
66. Guo, S.; Kong, L.-H.; Wang, P.; Yao, S.; Lu, T.-B.; Zhang, Z.-M. Switching Excited State Distribution of Metal-Organic Framework for Dramatically Boosting Photocatalysis. *Angew. Chem. Int. Ed.* **2022**, *61*, e202206193.

DOI: 10.31635/ccschem.024.202404675
Citation: *CCS Chem.* **2024**, 6, 3030–3040
Link to VoR: https://doi.org/10.31635/ccschem.024.202404675